EXTENDED EXPERIMENTAL PROCEDURES

Decolorization of the Blood by Aminoalcohols in CUBIC Cocktails

We hypothesized that CUBIC-1 reagent could solubilize and elute endogenous heme from blood-infused tissues. To test this hypothesis, we first investigated whether CUBIC reagents can directly decolorize blood. PFA-fixed blood was prepared by equivalent mixing of murine blood and 8% PFA-PBS, and incubated at 37°C overnight. Erythrocytes were purified by centrifugation of incoagulable blood including 1 mg/ml EDTA at 3000 rpm for 30 min, supernatant wasting, and followed by three-times washing with 1 ml PBS and centrifugation at 3000 rpm for 30 min. Both blood samples were stored at 4°C. In the decoloring experiments of PFA-fixed blood (Figures 1A and 1B), PFA-fixed blood (100 μl) was thoroughly mixed with each chemical [400 μl of PBS, CUBIC-1 reagent, 25 wt% *N,N,N′,N′*-tetrakis(2-hydroxypropyl)ethylenediamine (aminoalcohol #10), 25 wt% urea, 15 wt% Triton X-100, 0.01 M NaOH, the mixture of 25 wt% urea and 15 wt% Triton X-100, 25 wt% glycerol, or the mixture of 25 wt% urea, 25 wt% glycerol, and 15 wt% Triton X-100 (modified Sca*l*eA2)], and then immediately centrifuged at 15000 rpm for 5 min. Supernatant was collected and pellet was washed with each chemical (500 μl) three times (we noted that since mixing efficiency is critical for the clearing performance in the washing step, the mixture should be not only mixed by a vortex mixer, but also vigorously stirred by the small spatula). The pellet was suspended in each chemical (500 μl), and transferred in the dish. The collected supernatant (500 μl) was also transferred in the dish. Bright-field images of these samples were captured. As a result, aminoalcohol #10 alone, but not other reagents, is sufficient to decolorize the blood (Figure 1A). We also found that PFA-fixed blood could not be decolorized by glycerol, a mixture of urea and Triton X-100, or modified Sca*l*eA2 (the mixture of glycerol, urea, and Triton X-100) (Figure 1B), suggesting that aminoalcohol #10 in CUBIC-1 reagent is the active reagent in blood clearing. We also note that the decolorizing capability of aminoalcohol #10 is not solely dependent on its high pH because PFA-fixed blood was not efficiently decolorized by highly basic solution (0.01 M NaOH, initial pH = 12). Therefore, the blood decolorizing nature of aminoalcohol #10 in a moderately basic condition originates from its chemical property.

We next investigated what kind of olive-green molecule was eluted from the blood into the supernatant. Thus, the visible spectra of chemically-treated blood samples were recorded by UV/Vis spectrometer (JASCO, V-550) (Figures 1C, 1D, and S1A). Erythrocytes (5 μl) were mixed with each chemical (PBS, 0.1 M NaOH, 25 wt% #10, or CUBIC-1 reagent), and incubated at 37°C overnight. The mixtures and supernatant from CUBIC-1- or #10-treated PFA-fixed blood were diluted 10-fold with each chemical. We also prepared 10 μM of hemin (Tokyo Chemical Industry), 10 μM of biliverdin (Sigma-Aldrich), and 100μM of iron(II) chloride (Nacalai Tesque), solubilized with CUBIC-1 reagent or #10. The normalized spectra of the erythrocyte and supernatant overlapped almost completely with hemin solutions in aminoalcohol #10 or CUBIC-1, which suggests that heme is released from hemoglobin in erythrocytes when treated by aminoalcohol #10 or the CUBIC-1 reagent (Figures 1D and S1A).

Aminoalcohol #10 in the CUBIC-1 reagent can solubilize and elute the heme in the blood more efficiently than highly basic solution (0.01 M NaOH, initial pH = 12) (Figure 1A). What kind of chemical property in aminoalcohol #10 enables heme elution at moderate pH? As shown in Figure 1A, we noticed that the pH variations were relatively small between the original liquid and the subsequent supernatant for samples treated by aminoalcohol #10 and CUBIC-1 reagent when compared with highly basic solution (0.01 M NaOH, initial pH = 12). These results indicate that aminoalcohol #10 has buffering capacity at moderately basic conditions. To directly test the buffering capacity of these reagents, 50 g of CUBIC-1 reagent, 25 wt% aminoalcohol #10, 25 wt% glycerol containing 0.01 M NaOH, 25 wt% urea containing 0.01 M NaOH, 15 wt% Triton X-100 containing 0.01 M NaOH, or 0.01 M NaOH were titrated with 1 M HCl (Figure S1B). pH was measured by pH meter (HORIBA, LAQUAtwin). As a result, aminoalcohol #10 and CUBIC-1 reagent have buffering capacity in pH 9-11 whereas other reagents did not.

If buffering capacity in basic pH is critical for the decolorizing capability, we predicted that a basic solution containing 0.01 M NaOH, which usually elutes heme from hemoglobin, will lose its decolorizing capability at a higher concentration of erythrocytes because the higher concentration of cells will shift the pH from basic to neutral. To test this prediction, we prepared a mixture of erythrocytes and these chemicals at different ratios (Figure 1E). In the experiment, the mixtures (200 μl) of erythrocytes and each chemical (CUBIC-1 reagent, 25 wt% #10, 25 wt% glycerol containing 0.01 M NaOH, 25 wt% urea containing 0.01 M NaOH, 15 wt% Triton X-100 containing 0.01 M NaOH, or 0.01 M NaOH) with different mixing ratio (eryhtocyte/chemical = 0.01 to 0.20) were incubated at 37°C overnight. Bright-field images of these samples were captured. The OD575 and OD600 values of the mixtures were measured with the PowerWave XS and the attached operation software (Bio-Tek). Since the absorbance was saturated at erythrocyte/chemical ratio = 0.20 in Figure 1E, the OD600/OD575 values at this ratio were not collected in Figure S1C. These results quantitatively confirmed that aminoalcohol #10 in the CUBIC-1 reagent can efficiently promote heme release regardless of the erythrocyte/chemical ratio, and work as a decolorizing buffer at moderate basic pH.

Since previous studies reported that heme can be released only in highly basic (≥pH 11) or acidic (≤pH 2) conditions (Kristinsson and Hultin, 2004; Teale, 1959), the remaining question is whether the decolorizing capability of aminoalcohol #10 in the CUBIC-1 reagent occurs only in highly basic conditions (pH > 11), or can occur in less basic conditions (pH < 11), in which GFP-related fluorescence proteins emit stronger fluorescence signal (Haupts et al., 1998). Thus, we evaluated the pH dependence on the efficiency of heme release for 25 wt% aminoalcohol #10, CUBIC-1 reagent, 25 wt% tris(hydroxymethyl)aminomethane (Tris), and NaOH aqueous solution, respectively (Figure 1F). pHs of CUBIC-1 reagent, #10, Tris solutions were adjusted by acidification with HCl or basification with NaOH. Erythrocytes (5 μl) were mixed with each chemical (CUBIC-1 reagent, 25 wt% #10, 25 wt% Tris, or NaOH solution), and

incubated at 37°C for 1 hr. The OD575 and OD600 values of the mixtures were measured with the PowerWave XS. Haupts U. et al. revealed that GFP fluorescence signals were more intensified in the moderate basic condition (pH 8-11) than in the neutral condition (pH 7.0) (Haupts et al., 1998). In our previous manuscript, we also demonstrated that GFP signals in some of 10 wt% basic amino-alcohols were higher than those in PBS (pH 7.4) (Susaki et al., 2014). Therefore, moderate basic condition between pH 8 to 11 was optimal for fluorescence proteins. Additionally, aminoalcohol #10 has a strong buffering ability around pH 10 as shown in Figure S1B. Therefore, pHs in the medium could be kept between 10 to 11 through the CUBIC clearing protocol due to the daily exchange of the clearing medium. Actually, we showed the final pH values of the mixtures of erythrocyte and #10/CUBIC-1 were maintained over 10 as shown in the revised Figure 1E. Thus, we focused on the pH range between 9 to 13 in the experiment. In non-buffered basic solution, heme was efficiently released from hemoglobin, but only at pH > 11. On the other hand, aminoalcohol #10 efficiently eluted heme even in moderately basic conditions around pH 10. CUBIC-1 reagent further promoted heme release even around pH 9, which might be attributed to a combinatorial effect with urea and/or Triton X-100. These results suggested that aminoalcohol #10 in CUBIC-1 reagent expanded the pH window for efficient heme release.

To clarify the chemical properties of aminoalcohol #10 associated with its decolorizing capability, we investigated erythrocyte with a series of aminoalcohol derivatives (Figure S1E), which include primary amine (#8, #15, and Tris), secondary amine (#4), tertiary amine (#9, #10, #16, and #17) (Susaki et al., 2014) and amine bearing carboxylic acid groups (DHEG and EDTA) (Figure S1D). In the blood-decoloring by a series of aminoalcohol-related chemicals shown in Figure S1D, the mixtures were prepared according to the experiment of Figure 1E. Initial pH value in each chemical was pre-adjusted so that final pH ranges from 10.8 to 11.2. The decolorizing efficiency of primary amines is lower than those of secondary and tertiary amines (See also Figure 1F). Carboxylic groups also suppressed the decolorizing capability. These results revealed the chemical properties (i.e., higher amines without carboxylic groups) associated with efficient decolorizing and might reflect the affinity of these chemicals to the heme chromophore.

The reddish color of tissue originates mainly from the coordination of oxygen and histidine with heme in hemoglobin. Q bands (around 500-700 nm) of heme in erythrocytes treated with aminoalcohol #10 or CUBIC-1 reagent were considerably changed from those of hemoglobin-bound form (Figure 1C). Those were also different from Q bands of alkaline-denatured free form of heme. These results imply that the aminoalcohols could be tightly bound to heme porphyrin instead of oxygen and histidine in hemoglobin, which may facilitate heme release and explain the unexpected expansion of the effective pH window for heme release. We also found that secondary and tertiary amines with higher coordination capability than primary amines significantly decolorized the blood whereas related amines with a (charged) carboxyl group (DHEG and EDTA) exhibited less decolorizing capability (Figure S1D). We also note that the protonated (and hence charged) form of the aminoalcohol #10 (below its buffering pH ~10) decreased its decolorizing capability (Figure 1F). Since a heme molecule possesses an electron-deficient iron center and two negatively charged carboxyl groups, we speculated that uncharged aminoalcohol #10, which possesses highly coordinating tertiary amino groups, might have suitable chemical properties to efficiently coordinate to heme for blood decolorization.

In addition to this chemical property, the buffering capability of aminoalcohol #10 in moderately basic conditions should also contribute to the decolorizing performance. For example, hemoglobin has been usually quantified in basic Triton X-100 (pH > 13) because Triton X-100 could bind to heme in highly alkaline conditions (Wolf et al., 1984). However, the decolorization by basic Triton X-100 without buffering capability was not effective due to its variable pH (Figure 1E). Therefore, the buffering capability of aminoalcohol #10 will assist the release of heme either by Triton X-100 or aminoalcohol #10 itself. If aminoalcohol #10 did not have a buffering capability, the stable decolorizing capability may not be exerted (Figure 1F), as shown for Triton X-100 (Figure 1E). Importantly, the buffering capability of aminoalcohol #10 is exerted in moderately basic conditions, which is the optimal pH range for the fluorescence signal from GFP-related fluorescence proteins (Haupts et al., 1998). In fact, treatment of individual organs by CUBIC reagents led to much higher transmittance in the visible region than that of organs treated by other reagents (Figure S2B) while CUBIC reagents could preserve the fluorescence signal from various kinds of GFP-related fluorescence proteins (Figure S6). Taken together, two chemical properties (a heme-coordinating capability and a buffering capability in moderately basic conditions) contribute to decolorize the tissue and simultaneously preserve fluorescence signal from GFP-related fluorescence proteins.

Mice

The *β-actin-mKate2* knock-in mouse (β-actin-nuc-3 × mKate2) strain was established in our laboratory. A back-bone vector for targeting, pTVCI3, harboring all of the required elements, including the thymidine kinase (TK) promoter-driven cDNA encoding Diphtheria Toxin A-fragment (DT-A) from *ROSA26* targeting vector (Abe et al., 2011) and a synthetic sequence (5′-GCGGCCGCAGT TACGCTAGGGATAACAGGGTAATATAGGATCCCATTTCATTACCTCTTTCTCCGCACCCGACATAGATGATCCGTAACTATAACGGT CCTAAGGTAGCGAAGATCTGGCAAACAGCTATTATGGGTATTATGGGTGATCGAAAGAACCAGCTGGGGCTCGATCCCTCGAGAT CGGATATC-3′) as a multiple cloning region, was constructed by inserting these sequences at the *EcoR*V site of self-concatenated pGEM-T-Easy (Promega) after removal of potential cutting sites for *PI-Psp*I and *PI-Sce*I from pGEM-T-Easy. The multiple cloning region of resulting pTVCI3 contains *I-Sce*I, *PI-Sce*I, *I-Ceu*I, *PI-Psp*I, *Xho*I and *EcoR*V site as single restriction site, respectively. The 3′ homologous arm of *β-actin* was amplified from C57BL/6 mouse genomic DNA using PCR with the following primers: forward primer: (5′-CAGCTTGTGGCTCTGTGGCTTTGC-3′, Hokkaido System Science), reverse primer: (5′-ATGAAGAGATTGCTCAGTAGTTGAGA GAGTG-3′). PCR product was treated with Mighty Cloning kit (TaKaRa) for 5′-end phosphorylation, and cloned into the *EcoR*V site of pTVCI3, and the resulting vector was designated as pTVCI3-3arm. The 5′ homologous arm of *β-actin* was amplified

from C57BL/6 mouse genomic DNA using PCR with the following primers: forward primer: (5′-AACACCTCCAGTTATTGGACC ACTGG-3′), reverse primer: (5′-GTGCACTTTTATTGGTCTCAAGTCAGTG-3′). PCR product was treated with Mighty Cloning kit for 5′-end phosphorylation. pTVCI3-3arm was digested with *I-Sce*I (New England BioLabs), and blunted with T4 DNA polymerase (TaKaRa). The 5′ homologous arm fragment was ligated at the blunted *I-Sce*I site of pTVCI3-3arm, and designated as pTVCI3-5arm-3arm. pTVCI3-5arm-3arm was digested with *PI-Sce*I (New England BioLabs), blunted with T4 DNA polymerase. The Reading Frame Cassette B fragment from the Gateway Vector Conversion System (Life Technologies) was cloned into the blunted *PI-Sce*I site of pTVCI3-5arm-3arm, and the resulting vector was designated as pTVCI3-*β-actin*-GW. pTVCI3-*β-actin*-GW was mixed with pENTR-1A_CAG-nuc-3 × mKate2-WPRE-PuroR (Susaki et al., 2014) to perform the LR recombination reaction using the Gateway LR Clonase II Enzyme mix (Life Technologies). In the resulting targeting vector, the insertion cassette was in the same orientation as the *β-actin* gene.

C-terminal-truncated (+63) TALENs (Miller et al., 2011) that bind target sequence (5′-*GGCCTGTACACTGACTT*GAGACCAA TAAAAGTGC*ACACCTTACCTTACAC*-3′, TALEN binding sequences are indicated with italics) containing a polyadenylation signal sequence were designed using TALE-NT (Doyle et al., 2012). The targeting vector and TALEN-expression vector were purified and introduced into HK3i C57BL/6 mouse embryonic stem (ES) cells (Kiyonari et al., 2010) using Xfect Transfection Reagent (Clontech Laboratories, Inc. A Takara Bio Company) according to the manufacturer's instructions, and the homologous recombined, puro-resistant ES cell clones were isolated for further culture and expansion. An aliquot of the cells was lysed and screened for successful homologous recombination by PCR. The integrity of the targeted region was confirmed by PCR using primers annealing outside the homologous recombination arms and within the inserted cassette. The primers used for the screening and the confirmation of genome integrity were as follows: 1) forward primer annealing to the region upstream of the 5′ homologous arm: 5′-CTGGCAGT CACCCAGAGACACTAGC-3′, 2) reverse primer annealing to the region downstream of the 5′ homologous arm: 5′-GTTAGTGCA GGCCAACTTGGCCTAGG-3′, 3) forward primer annealing to the region upstream of the 3′ homologous arm: 5′-AGGATGG TCGCGTCCATGCCCTGAG-3′, 4) reverse primer annealing to the region downstream of the 3′ homologous arm: 5′-ACTTCCAGGA GCCCTATGTGGTAGC-3′, 5) reverse primer annealing to the region between 5′ homologous arm and Gateway cassette of pTVCI3: 5′-GGTAATGAAATGGGATCCTATATTACCC-3′, and 6) forward primer annealing to the region between 3′ homologous arm and Gateway cassette of pTVCI3: 5′-GAAAGAACCAGCTGGGGCTCGATCC-3′. The copy number of the inserted cassette was confirmed with a quantitative PCR assay using primers annealing to the coding sequences of the puro-resistance gene (forward primer: 5′-CTCGACATCGGCAAGGTGTG-3′, reverse primer: 5′-GGCCTTCCATCTGTTGCTGC-3′) (Susaki et al., 2014), normalized to the amount of TATA-box binding protein gene amplification (forward primer: 5′-CCCCCTCTGCACTGAAATCA-3′, reverse primer: 5′-GTAGCAGCACAGAGCAAGCAA-3′) (Tsujino et al., 2013) using the SYBR Premix Ex Taq GC (TaKaRa) and the ABI PRISM 7900 (Applied Biosystems). The selected ES cell clones were injected into 8-cell-stage ICR embryos to generate ~100% ES cell-derived chimeras (Kiyonari et al., 2010).

We also used the R26-H2B-EGFP (CDB0238K) mouse strain (Abe et al., 2011), the Thy1-YFP-H transgenic mouse strain (Feng et al., 2000), the R26-pCAG-nuc-3 × mKate2 mouse strain (Susaki et al., 2014), and the C57BL/6-Tg (CAG-EGFP) mouse strain (Okabe et al., 1997) to observe static fluorescent gene-expression patterns in whole-organ imaging. Mouse strains were maintained in the C57BL/6 background. We purchased the BALB/cAJcl-*nu/nu* mouse strain from CLEA Japan, Inc. and the C57BL/6-Tg (CAG-EGFP) mouse strain from Japan SLC, Inc.

All experimental procedures and housing conditions were approved by the Animal Care and the Use Committee of Graduate School of Medicine, the University of Tokyo or by the Animal Care and Use Committee of the RIKEN Kobe Institute and all of the animals were cared for and treated humanely in accordance with the Institutional Guidelines for Experiments using animals. We fed DietGel Recovery (LSG Corporation, 72-06-5022, Japan) to mice for imaging the intestine.

Mouse Model of Streptozotocin (STZ)-Induced Diabetes

Diabetes was induced in male C57BL/6N mice at 8 weeks by a single intraperitoneal administration of saline (Otsuka Pharmaceutical Co., Ltd., 14987035081514, Japan) or 10 mg/ml streptozotocin (total 200 mg/kg, Wako Pure Chemical Industries, Ltd., 197-15153, Japan) dissolved in saline at day 0. At day 0 and day 4, blood glucose values were measured by a blood glucose monitor (GLUCOCARD G Black; ARKRAY, Inc., Japan) after fasting for 6 hr. Body weight was also measured at the same days. After four days, blood sugar levels of 36% of the mice were elevated over 300 mg/dl, which is a commonly-used criterion for the diagnosis of diabetes (Table S1). Mice with blood glucose levels over 300 mg/dl (n = 5) at day 4 and saline-administered mice (n = 4) were used for clearing with CUBIC (CB)-perfusion and PI staining. Imaging was performed using mice with the highest blood glucose levels of STZ group (n = 3) and corresponding number of control group (n = 3).

Comparison of Clearing Methods

A number of tissue-clearing methods (including BABB, THF-DBE, Sca*l*e, SeeDB, *Clear*^{T}, 3DISCO, CLARITY, CUBIC, and PACT-PARS) have been intensively developed. Because a simple and versatile protocol will facilitate a high-throughput approach to understanding cellular circuits in organisms, we mainly focused on the development of an immersion-only tissue-clearing protocol. Organic solvent-based clearing media such as BABB, THF-DBE decrease signals from fluorescent proteins with short duration (Ertürk et al., 2012; Hama et al., 2011). In addition, benzylalcohol and THF inherently generates potentially explosive peroxide and this also quenches the fluorescence signals of fluorescent proteins (Alnuami et al., 2008). Therefore, peroxides in benzylalcohol and THF

have to be removed by specific apparatus before use. Although organic solvent based clearing medium remains to be attractive in the clearing performance, these experimental drawbacks compelled us to focus on water-based clearing reagents. For Figure 2A, we compared four chemical-based clearing methods. For collecting organ samples, adult mice (C57BL/6N and BALBc-*nu/nu*) were sacrificed by an overdose of pentobarbital (>100 mg/kg, Kyoritsu Seiyaku, Japan) and then perfused with 10 ml of 10 U/ml of heparin (Wako Pure Chemical Industries, 081-00136) in PBS (pH 7.4) and 20 ml of 4% (w/v) paraformaldehyde (PFA, Nacalai Tesque, 02890-45) in PBS via left ventricle of the heart. The excised organs (brain, heart, lung, right lobe of the liver, both side of the kidneys, pancreas, spleen, stomach, intestine, triceps surae muscle and skin) were post-fixed in 4% (w/v) PFA for 24 hr at 4°C. The specimens were washed with PBS for 20 min x three times to remove PFA just before clearing. Uncleared organs (negative control) were stocked in PBS with 0.01% Sodium Azide (Nacalai Tesque, 31208-82) at 4°C after fixation. In SeeDB standard protocol (Ke et al., 2013), the fixed organs were serially rotated (4 rpm) in 30 ml of 20%, 40%, 60% (w/v) fructose (Nacalai Tesque, 16315-55) for 8 hr each and in 30 ml of 80%, 100% (w/v) fructose for 12 hr each. From day 3, these organs were rotated in 30 ml of SeeDB (80.2% w/w fructose) at 25°C. SeeDB solution was replaced to the fresh one every day until observation. All fructose solutions contained 0.5% α-thioglycerol (Tokyo Chemical Industry, S0374). In Sca*l*eA2 and Sca*l*eB4 protocol (Hama et al., 2011), the fixed organs were immersed in 20% (w/v) sucrose (Nacalai Tesque Inc., 30403-55, Japan) at 4°C for 24 hr. These organs were embedded in OCT compound (Sakura Finetek Japan Co., Ltd., 4583) and frozen at −80°C. The next day, they were thawed in PBS and fixed again in 4% PFA. From day 3, these organs were rotated in 30 ml of Sca*l*eA2 (4 M urea, Nacalai Tesque, 35904-45, 10% (w/v) glycerol, Nacalai Tesque, 17018-25, and 0.1% (v/v) Triton X-100, Nacalai Tesque, 25987-85) for 2 days, 30 ml of Sca*l*eB4 (8 M urea, 0.1% (v/v) Triton X-100) for 2 days, and 30 ml of Sca*l*eA2 for 3 days in this order. All of the Sca*l*e solutions were replaced to the fresh one every day until observation. Two CUBIC reagents were prepared as previously reported (Susaki et al., 2014). Aminoalcohol #10 [*N,N,N′,N′*-tetrakis(2-hydroxypropyl) ethylenediamine (Tokyo Chemical Industry, T0781)] is a constituent of previously published CUBIC-1 chemical cocktail. Aminoalcohol #16 [2,2′,2″-nitrilotriethanol (Wako Pure Chemical Industries, 145-05605)] is a constituent of previously published CUBIC-2 chemical cocktail. In brief, Sca*l*eCUBIC-1 (CUBIC-1 reagent) was prepared as a mixture of 25 wt% urea, 25 wt% aminoalcohol #10, and 15 wt% Triton X-100. Sca*l*eCUBIC-2 (CUBIC-2 reagent) was prepared as a mixture of 50 wt% sucrose, 25 wt% urea, 10 wt% aminoalcohol #16, and 0.1% (v/v) Triton X-100. We adopted two CUBIC protocols for this comparing experiment. For preparation of CUBIC-treated (non-perfused) samples, the fixed organs (from C57BL/6N) and skin (BALBc-*nu/nu,* to save plucking hairs before clearing) were immersed in 30 ml of CUBIC-1 reagent at 37°C with gentle shaking for 5 days. These organs were then washed with PBS and immersed in 50% glycerol at room temperature on day 6. They were immersed in 30 ml of CUBIC-2 reagent at room temperature on day 7 and at 37°C after day 8. In all four clearing methods, stomach and intestine were separately immersed from other organs to avoid contamination of sticky gastrointestinal contents.

To make CUBIC-1 reagent penetrate throughout the whole body, we also performed the CUBIC (CB)-Perfusion protocol as follows; the anesthetized mouse was perfused with 10 ml of 10 U/ml of heparin in PBS, 150 ml of 4% (w/v) PFA in PBS, 20 ml of PBS (to wash out PFA), and 20 ml of 50% (v/v) CUBIC-1 reagent (1: 1 mixture of water: CUBIC-1 reagent) in this order via left ventricle of the heart. The resulted organs were excised and continuously immersed in 30 ml of CUBIC-1 reagent at 37°C with gentle shaking for 5 days. These organs were washed with PBS, immersed in 50% glycerol in PBS at room temperature on day 5. Then, they were immersed in 30 ml of CUBIC-2 reagent at room temperature on day 6 and at 37°C after day 7. Bright-field images of adult mice (19-week-old) demonstrated that CB-Perfusion protocol markedly transparentized and decolorized adult mice (Figures 2B and S2C). Since the abdominal organs of adult mouse (including liver, pancreas, spleen, stomach, and small and large intestines) were sufficiently transparentized and decolorized, the backbones (the lumbar and sacrum vertebrae) and pelvis were easily visualized even in the ventral-to-dorsal (V-D) image of adult mice (Figure 2B). Similarly, the chest organs of adult mouse (including lung, heart, aorta, pulmonary artery and bronchi) were also highly transparentized and decolorized. Hence, the backbones (the cervical and thoracic vertebrae) and entire rib cages were easily visualized even in the ventral-to-dorsal (V-D) image of adult mice (Figure 2B). Furthermore, the muscles of limbs in adult mouse were markedly transparentized and decolorized. Therefore, the bones of forelimbs (including scapula, humerus, radius and ulna) and hindlimbs (including femur, tibia and fibula), and caudal vertebrae were clearly visualized in either V-D or the dorsal-to-ventral (D-V) images of adult mice (Figures 2B and S2C).

Measurement of Light Transmittance

For Figures S2A and S2B, we measured light transmittance of the brain, heart, lung, liver and kidney samples use in Figure 2A, from 380 to 780 nm at 5 nm intervals with an integrating sphere (Spectral Haze Meter SH 7000, Nippon Denshoku Industries). We put every sample in the center of the optical cell (Nippon Denshoku Industries, 2277) without liquid to avoid sample floating. Finally, the height of the sample and the aperture of integrating sphere were adjusted before measurement.

In the instrument, two values can be determined: (1) diffused (scattered) light transmittance (%) which is the value for the light transmitted through the tissue, (2) parallel (non-diffused) light transmittance (%) which is the value for the light detected without any prevention. Diffused light transmittance was calculated as the value of (total light transmittance – parallel light transmittance) in the integrating sphere. We also calculated (100 – parallel light transmittance) as a tissue size-related value, because the sample makes a 'shadow' over the parallel light detector and the 'shadow' size is related to the sample size. Thus, the final transmittance was calculated by the diffused light transmittance divided by the value of (100 – parallel light transmittance) to be compensated with the tissue size and compared directly even between the values from different tissues. Finally, the final transmittance from four samples was averaged.

The CUBIC Protocol for Whole-Body and -Organ Imaging

For whole body and organ imaging, we slightly modified the above CUBIC protocol to improve the transparency and quality of imaging data (Figures 2B, 3, and 4).

For whole body imaging, adult (6 – 19 weeks old) mouse were subjected to the same CB-Perfusion protocol as above, and then the CB-perfused mouse was immersed in 200 ml of CUBIC-1 reagent at 37°C with gentle shaking for at least two weeks. To facilitate the whole-body clearing, the reagent was refreshed daily for two weeks. The clearing medium gradually became less colored, and after two weeks the apparent transparency of the whole body became saturated. Whole-body samples can be then stored in CUBIC-1 reagent, and even shaken in 37°C over months until observation because the high pH of CUBIC-1 reagents prevents proliferation of microorganisms. The resulted sample was used for imaging and thus we did not perform further clearing with CUBIC-2 reagent.

For whole organ imaging, adult mice were subjected to the CB-Perfusion protocol as above. Organs were excised and continuously immersed in 30 ml (stomach, intestine) or 60 ml (brain, heart, lung, liver, kidneys, pancreas, spleen, muscle) of CUBIC-1 reagent at 37°C with gentle shaking at least for 7 days. To facilitate the clearing, the reagent was refreshed daily for one week, and the transparency was saturated within 10 days as in Figure 2 and S2. The samples can be then stored in CUBIC-1 reagent, and even shaken in 37°C over weeks to months to prevent proliferation of microorganisms as above. These organs were washed with PBS, immersed in 50% glycerol in PBS at room temperature, and then they were immersed in 30 ml of CUBIC-2 reagent for each group at room temperature on the first day and at 37°C after the second day. Images were acquired after 3 days incubation in CUBIC-2 reagent. For skin imaging in Figure 4E, a CAG-EGFP Tg mouse (10-week-old) was also subjected to CB-Perfusion as above. The excised skin and ear were needed to remove subcutaneous tissues and hairs, and thus we washed the specimens with PBS several times and then post-fixed and cleared according to non-perfusion protocol as above 10-day protocol. Images were acquired on day 12.

The 3D reconstitution image of heart from SYTO 16-stained nuc-3 × mKate2 demonstrated that SYTO 16 signals highlighted epicardium, papillary muscle, and right atrium whereas mKate2 signal was higher in coronary vessels (Figure 4A). The expression level of mKate2 is dependent on the cell type in each tissue because mKate2 is expressed under the control of CAG promoter in ROSA26 locus, and therefore distribution of the mKate2 fluorescent signals reflected the expression of the knocked-in expression cassette. On the other hand, SYTO 16 indiscriminately stained all cell nuclei in the tissue. Thus, distribution of the SYTO 16 fluorescent signals was attributed to the cell density in each tissue. The spatial distribution of fluorescence proteins (EGFP in Figure S6A and nuc-3 × mKate2 in Figures 4 and S5) was also markedly different. This is because EGFP was localized in the nucleus and cytosol whereas mKate2 was localized only in the nucleus. Therefore, EGFP signals were useful for the visualization of the orientation of muscular fibers in heart and muscle, whereas mKate2 signals could highlight the vascular and duct structures in heart, kidney, pancreas, and spleen. In addition, expression levels of these fluorescence proteins varied in each organ. For example, EGFP signals were more intense in the heart and the pancreas whereas mKate2 signals were elevated in the brain, the kidney, and the pancreas.

For a neonatal (postnatal day 1 or day 6) mouse clearing, 3 ml of 10 U/ml of heparin in PBS, 10 ml of 4% (w/v) PFA in PBS, 3 ml of PBS and 5 ml of 50% (v/v) CUBIC-1 reagent were perfused in this order via left ventricle of the heart after the anesthetization. Furthermore, 3 ml of CUBIC-1 reagent were additionally perfused for improving the transparency. Gastrointestinal tract was also flushed with CUBIC-1 reagent from the mouth. The mouse was then immersed in 30 ml of CUBIC-1 reagent at 37°C with gentle shaking for at least 2 weeks. To facilitate the clearing, the reagent was refreshed daily for two weeks. The samples can be then stored in CUBIC-1 reagent, and even shaken in 37°C over weeks to months to prevent proliferation of microorganisms as above. This sample was used for imaging and thus we did not perform further clearing with CUBIC-2 reagent. In the whole body imaging of P1 mouse, we noted that PI fluorescence signal was enhanced where it binds not only with DNA in the nucleus of internal organs and soft tissues but also in bone tissues (Figure 3A). Although light-sheet illumination was shaded to some extent by bone-rich structures such as paws, fluorescence signal from shaded regions was still detectable. According to the whole-body images, organ transparency was not diminished through the whole-body clearing procedure compared to clearing of individual organs separately.

Whole body and organs were stained with nucleic acid stain (propidium iodide (PI), life technologies, P21493 or SYTO 16, Life Technologies, S7578), added in 50% (v/v) CUBIC-1 reagent (for CB-Perfusion), CUBIC-1 and -2 reagents (during clearing) at a concentration of 10 μg/ml PI or 0.5 μM SYTO16, when indicated. Note that 50% (w/v) Glycerol in PBS used before CUBIC-2 reagent can be exchanged with 20% (w/v) sucrose in PBS in the original brain clearing protocol (Susaki et al., 2014).

Microscopy

Whole-body and organ fluorescence images were acquired with light-sheet fluorescence microscopy (LSFM) (Ultramicroscope, LaVision BioTec) as reported previously (Dodt et al., 2007; Susaki et al., 2014). Samples were immersed in a 1:1 mixture of silicon oil TSF4300 (Momentive Performance Materials, RI = 1.498) and mineral oil (Sigma-Aldrich, RI = 1.467), and were put on a glass plate held with a customized sample holder. Images were captured at 0.63 × to 5 × zoom with the MVX-ZB10. Each plane was illuminated from both the right and left sides, and a merged image was saved. The exposure times were adjusted according to the fluorescent signal intensities of each sample. Detailed imaging conditions in each figure described as below; Figure 3 (A) Z-stack: 20-μm step, with 4.0 s × two illuminations for EGFP and with 0.1 s × two illuminations for PI. Zoom of the microscope: 0.63 ×, (B) Z-stack: 20-μm step, with 4.0 s × two illuminations for EGFP and with 0.1 to 0.15 s × two illuminations for PI. Zoom of the microscope: 2.0 × except 2.5 × for chest V-D images, (C) Z-stack: 20-μm step, with 0.4 to 2.0 s × two illuminations for EGFP and with 0.1 to 0.2 s × two illuminations for PI. Zoom of the microscope: 0.8 × except 1.25 × for chest V-D images, Figure 4 (A) Heart images. Z-stack: 20-μm step × 346 planes, with 0.05 s × two illuminations for SYTO 16 and with 0.5 s × two illuminations for mKate2. Zoom of

the microscope: 2.0 × . (B) Lung images. Z-stack: 20-μm step × 306 planes, with 0.05 s × two illuminations for SYTO 16 and with 1.0 s × two illuminations for mKate2. Zoom of the microscope: 1.0 × . (C) Kidney images. Z-stack: 20-μm step × 256 planes, with 0.05 s × two illuminations for SYTO 16 and with 0.5 s × two illuminations for mKate2. Zoom of the microscope: 1.6 × . (D) Liver images. Z-stack: 20-μm step × 266 planes, with 0.05 s × two illuminations for SYTO 16 and with 0.5 s × two illuminations for mKate2. Zoom of the microscope: 1.0 × . (E) Skin and ear images. Z-stack: 20-μm step, with 0.2 to 0.5 s × two illuminations for EGFP and with 0.1 s × two illuminations for PI. Zoom of the microscope: 1.6 × for ear, 2.0 × for skin, and 6.3 × for both magnified images, Figure 7 (B) Heart images. Z-stack: 10-μm step × 501 planes (whole image) or × 201 planes (magnified image), with 0.1 s × two illuminations or 0.1 s × single illumination for SYTO 16 and with 2.0 s × two illuminations or 3.0 s × single illumination for Cy3, respectively. Zoom of the microscope: 2.5 × or 6.3 × . (C) Lung images. Z-stack: 10-μm step × 511 planes (whole image) or × 101 planes (magnified image), with 0.1 s × two illuminations or 0.2 s × two illuminations for PI and with 2.0 s × two illuminations or 3.0 s × two illuminations for FITC, respectively. Zoom of the microscope: 1.6 × or 6.3 × . (D) Stomach images. Z-stack: 10-μm step × 381 planes (whole image) or × 167 planes (magnified image), with 0.1 s × two illuminations or 0.1 s × single illumination for SYTO 16 and with 1.0 s × two illuminations or 1.0 s × single illumination for Cy3, respectively. Zoom of the microscope: 2.0 × or 6.3 × . (E) Intestine images. Z-stack: 10-μm step × 371 planes (whole image) or × 101 planes (magnified image), with 0.1 s × two illuminations or 0.1 s × single illumination for SYTO-16 and with 2.0 s × two illuminations or 3.0 s × single illumination for Cy3, respectively. Zoom of the microscope: 1.25 × or 6.3 × .

Image Data Processing and Analysis

All raw image data were collected in a lossless 16-bit TIFF format. 3D-rendered images were visualized and captured with Imaris software (version 7.6.4 and 7.7.1, Bitplane). Brightness, contrast, and gamma of the 3D-rendered images were manually adjusted with the software at minimum when visualized.

We performed blind 3D deconvolution for a set of our LSFM Z-stack images with software AutoQuant X3 (Media Cybernetics). Because the software does not have a preset for a macrozoom LSFM images, we searched parameters to significantly improve the raw tiff images. Using the expert settings, we performed the 3D blind deconvolution with 50 iterations, noise manually set to 0, and the original unfiltered image as initial guess. Montage was used both in the XY and Z directions, with 15-pixel sub-volume overlap. RIs were to 1.00 and 1.49, with lens aperture at 0.15. Spacing, wavelength and magnitude settings are sample-dependent, and all other parameters were kept to the default values for the ''multi-photon fluorescence'' modality. Results were saved as 16-bit tiff images.

The reconstituted 3D images were then used for image analysis with Imaris software (Bitplane). In order to reliably identify all LIs in the pancreas, we acquired 6-10 sets of the magnified z-stack images to cover the entire pancreas. LIs were identified as dense clusters of PI-stained cellular nuclei in the magnified images. These images also enabled us to morphologically distinguish the characteristic clusters (LIs) from the characteristic tracts (pancreatic ducts) (Figure 5A). We identified all LIs by visual annotation of all z-stack planes in all sets of magnified images of a pancreas. The extracted LIs were then 3D-reconstituted by the surface analysis in the Imaris software. For example, yellow (in the indicated z-stack plane) and blue objects (outside the indicated z-stack plane) indicate LIs whereas green objects indicate pancreatic ducts (Figure 5A). We thus performed comprehensive and statistical analysis of diabetic LIs in the whole-pancreas of adult mice (Figure 5B). For the visualization of anatomical structures (Figures 6, S7, and S8), we selected appropriate analytical segments in each organ and manually extracted signal intensities correlated with these structures on the Surface analysis of the software. Then, each structure was manually curated and extra Surface signals were eliminated.

For extraction, counting, and volume calculation of pancreatic islets, pancreases derived from the STZ experiment and cleared by CB-Perfusion with PI staining were used. Whole-tissue 3D images of each pancreas were acquired as 6 to 10-divided region images with 4 × zoom of MVX10. The merged areas were annotated manually. Each islet was morphologically detected in the entire X-Y plane images. Then, a 3D region including one to three islets was selected for Surface analysis of Imaris software. The size of automatically selected Surface was manually adjusted to the actual islet size by changing Threshold (Absolute intensity) parameter. To remove Surfaces other than islet, Volume parameter was changed to 10^3 or 10^4 voxel number (depending on the islet size of the selected region), and manually removed the remaining Surfaces other than islet. Number and volume of islets were calculated by Imaris. Further statistical analyses between saline- or STZ- administered groups were performed using R software (Kolmogorov-Smirnov test for difference in islet size distribution, and comparison of total islets, islets larger or smaller than 1.0×10^7 μm^3 for t test).

As a pilot study, we considered the automatic extraction of relevant anatomical structures in the heart and pancreas. For heart samples, analysis is performed in Fiji (Schindelin et al., 2012). We successively run the ''Smooth'' and ''Find Edges'' methods, followed by the ''Tubeness'' plugin (with sigma = 1). Finally, we apply a binary mask to keep only pixels with intensity higher than 400. As shown in Figure S7B, the method successfully extracts coronary arteries and most of them were merged to the manual extracted Surface signal in Imaris. For the pancreas samples, the objective is to accelerate the identification of Langerhans islets. Our method relies on two properties of these islets: (a) even though their intensity varies, the islets are generally brighter than their immediate surroundings; (b) islets have a roughly spherical shape. The first property is used in the pre-processing method, implemented in C++. Using a sliding window, we measure the average intensity in each region of each Z-slice of the 3D image, and only keep pixels with intensity at least 10% higher than this local average. All other pixels are set to 0. Each pre-processed 2D slice is then analyzed in Fiji. We run the ''Find Edges'' method, followed by computing of the largest absolute eigenvalue of the Hessian matrix (using the corresponding FeatureJ plugin with smoothing = 1), to identify clusters that do not have the desired shape. At each pixel, the eigenvalue

is then multiplied by seven and subtracted from the current intensity. We save the resulting file for each slice, and re-construct the 3D image. While the method still needs to be refined, early results on the clearest slices are encouraging (Figure 5C). For darker slices, curation of the result file removes inaccurate annotations. This process will be automatized in future versions.

3D Immunostaining of CUBIC Samples

3D IHC protocol for CUBIC samples was according to our previous paper (Susaki et al., 2014). Organ samples with CB-Perfusion were treated with CUBIC-1 for 7 days, washed with PBS, immersed in 20% (w/v) sucrose in PBS, and frozen in O.C.T. compound at –80°C overnight. The frozen samples were then thawed, washed with PBS, and subjected to immunostaining with the 1:100 diluted fluorescent-labeled antibodies in 5 ml of 2% (v/v) Triton X-100 in PBS for 3 days at 4°C with rotation. The stained samples were then washed with 5 ml of PBS several times at 37°C with rotation. The stained samples were then immersed in CUBIC-2 for 4 to 15 hr. The following antibodies were used for the staining: Cy3-conjugated anti-α-smooth muscle actin (α-SMA) antibody produced in mouse (Sigma, C6198) for heart, stomach, and intestine, and monoclonal FITC-conjugated anti-Pan cytokeratin antibody [C-11] (abcam, ab78478) for lung. These antibodies were mixed with the samples after filtration with an Ultrafree-MC GV Centrifugal Filter (Millipore UFC30GV00).

SUPPLEMENTAL REFERENCES

Doyle, E.L., Booher, N.J., Standage, D.S., Voytas, D.F., Brendel, V.P., Vandyk, J.K., and Bogdanove, A.J. (2012). TAL Effector-Nucleotide Targeter (TALE-NT) 2.0: tools for TAL effector design and target prediction. Nucleic Acids Res. *40* (Web Server issue), W117–W22.

Kiyonari, H., Kaneko, M., Abe, S., and Aizawa, S. (2010). Three inhibitors of FGF receptor, ERK, and GSK3 establishes germline-competent embryonic stem cells of C57BL/6N mouse strain with high efficiency and stability. Genesis *48*, 317–327.

Miller, J.C., Tan, S., Qiao, G., Barlow, K.A., Wang, J., Xia, D.F., Meng, X., Paschon, D.E., Leung, E., Hinkley, S.J., et al. (2011). A TALE nuclease architecture for efficient genome editing. Nat. Biotechnol. *29*, 143–148.

Tsujino, K., Narumi, R., Masumoto, K.H., Susaki, E.A., Shinohara, Y., Abe, T., Iigo, M., Wada, A., Nagano, M., Shigeyoshi, Y., and Ueda, H.R. (2013). Establishment of *TSH* β real-time monitoring system in mammalian photoperiodism. Genes Cells *18*, 575–588.

Wolf, H.U., Lang, W., and Zander, R. (1984). Alkaline haematin D-575, a new tool for the determination of haemoglobin as an alternative to the cyanhaemiglobin method. II. Standardisation of the method using pure chlorohaemin. Clin. Chim. Acta *136*, 95–104.

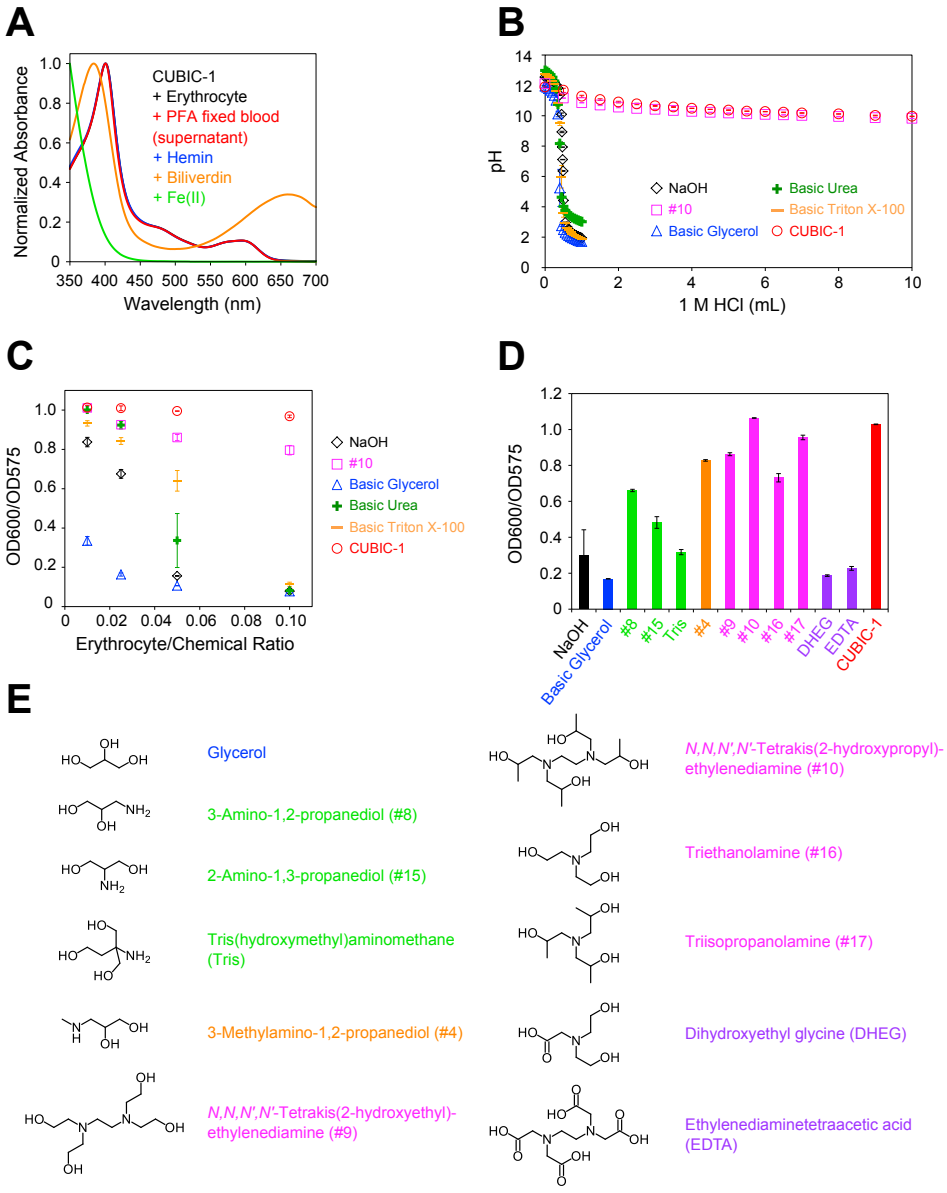

Figure S1. Aminoalcohols in CUBIC Cocktails Decolorized the Blood by Efficiently Eluting Heme Chromophore, Related to Figure 1

(A) Normalized visible spectra of 0.1% mouse erythrocyte (black), 1/10 diluted supernatant from Figure 1A (red), 10 μM hemin (blue), 10 μM biliverdin (orange), and 100 μM iron(II) chloride (green), in CUBIC-1 reagent.

(B) 50 g of CUBIC-1 reagent (red circle, n = 3), 25 wt% aminoalcohol #10 (magenta square, n = 3), 25 wt% basic glycerol (blue triangle, n = 3), 25 wt% basic urea (green cross, n = 3), 15 wt% basic Triton X-100 (orange bar, n = 3), or 0.01 M NaOH (black diamond, n = 3) were titrated with 1 M HCl. pHs are plotted against the titrated volume of 1 M HCl. Data represent the average ± SD.

(C) OD600/575 values of 1% to 20% erythrocyte solution mixed with CUBIC-1 reagent (red circle, n = 3), 25 wt% aminoalcohol #10 (magenta square, n = 3), 25 wt % basic glycerol (blue triangle, n = 3), 25 wt% basic urea (green cross, n = 3), 15 wt% basic Triton X-100 (orange bar, n = 3), and 0.01 M NaOH (black diamond, n = 3) in Figure 1E are plotted against erythrocyte/chemical mixture ratio. Data represent the average ± SD.

(D) OD600/575 values of 1% erythrocyte solution mixed with a series of aminoalcohols [primary amine (green, n = 3), secondary amine (orange, n = 3), tertiary amine (magenta, n = 3), or amine bearing carboxylic acid (purple, n = 3)], NaOH (black, n = 3), basic glycerol (blue, n = 3) or CUBIC-1 reagent (red, n = 3) is shown. Initial pH value in each chemical was pre-adjusted so that final pH ranges from 10.8 to 11.2. Data represent the average ± SD.

(E) Chemical structures of glycerol and a series of aminoalcohols examined in this study. Numbering of the chemicals was derived from the previous chemical screening. Glycerol is a polyhydric alcohol without an amine group. 3-Amino-1,2-propanediol (#8), 2-amino-1,3-propanediol (#15), and tris(hydroxymethyl) aminomethane (Tris) are aminoalcohols with primary amine. 3-Methylamino-1,2-propanediol (#4) is a aminoalcohol with a secondary amine group. *N,N,N′,N′*-Tetrakis(2-hydroxyethyl)ethylenediamine (#9), *N,N,N′,N′*-tetrakis(2-hydroxypropyl)ethylenediamine (#10), triethanolamine (#16), and triisopropanolamine (#17) are aminoalcohols with a tertiary amine group. Dihydroxyethyl glycine (DHEG) and ethylenediaminetetraacetic acid (EDTA) are amines with carboxylic groups.

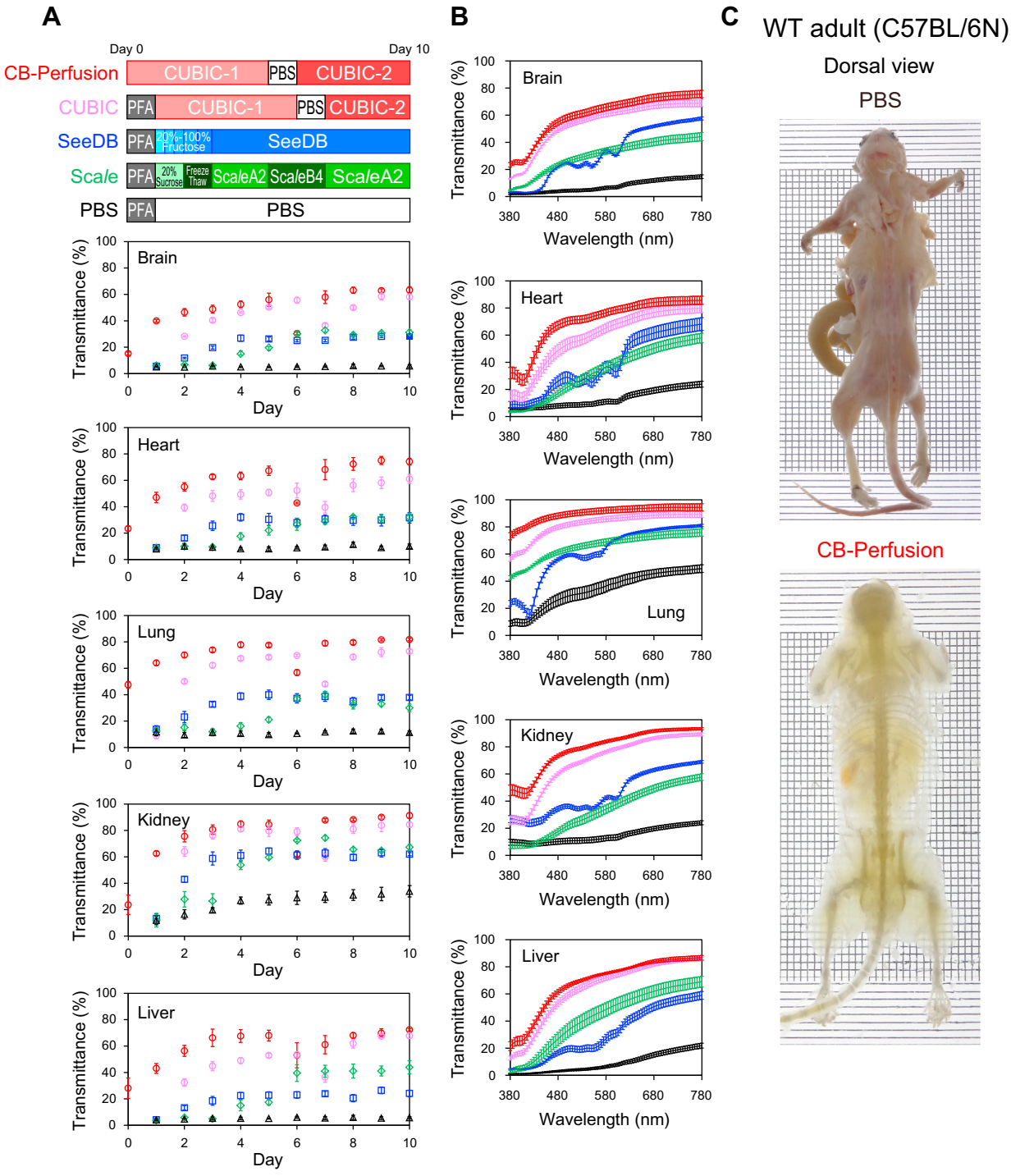

Figure S2. CUBIC Is a Simple and Efficient Whole-Organ and Whole-Body Clearing Protocol, Related to Figure 2

(A) Temporal development of transmittance of different organs (brain, heart, lung, kidney, and liver) with each protocol. Average light transmittance of fixed whole organs treated with PBS (black, n = 4), the *Sca/e* protocol (green, n = 4), the SeeDB protocol (blue, n = 4), the CUBIC protocol (pink, n = 4) or the CB-Perfusion protocol (red, n = 4), were measured. Data represent the average ± SD.

(B) Transmission curves of different organs (brain, heart, lung, kidney, and liver) with each protocol after 10 days. Light transmittance around the visible region (380-780 nm) of fixed whole organs treated with PBS (black, n = 4), *Sca/e* protocol (green, n = 4), SeeDB protocol (blue, n = 4), CUBIC protocol (pink, n = 4) or the CB-Perfusion protocol (red, n = 4) were measured. Data represent the average ± SD.

(C) Bright-field images (dorsal view) of fixed whole body (C57BL/6N adult mice) stocked in PBS or subjected to the CB-Perfusion protocol, also shown in Figure 2B. 8-week-old mouse for the PBS sample and 19-week-old mouse for the cleared sample are shown.

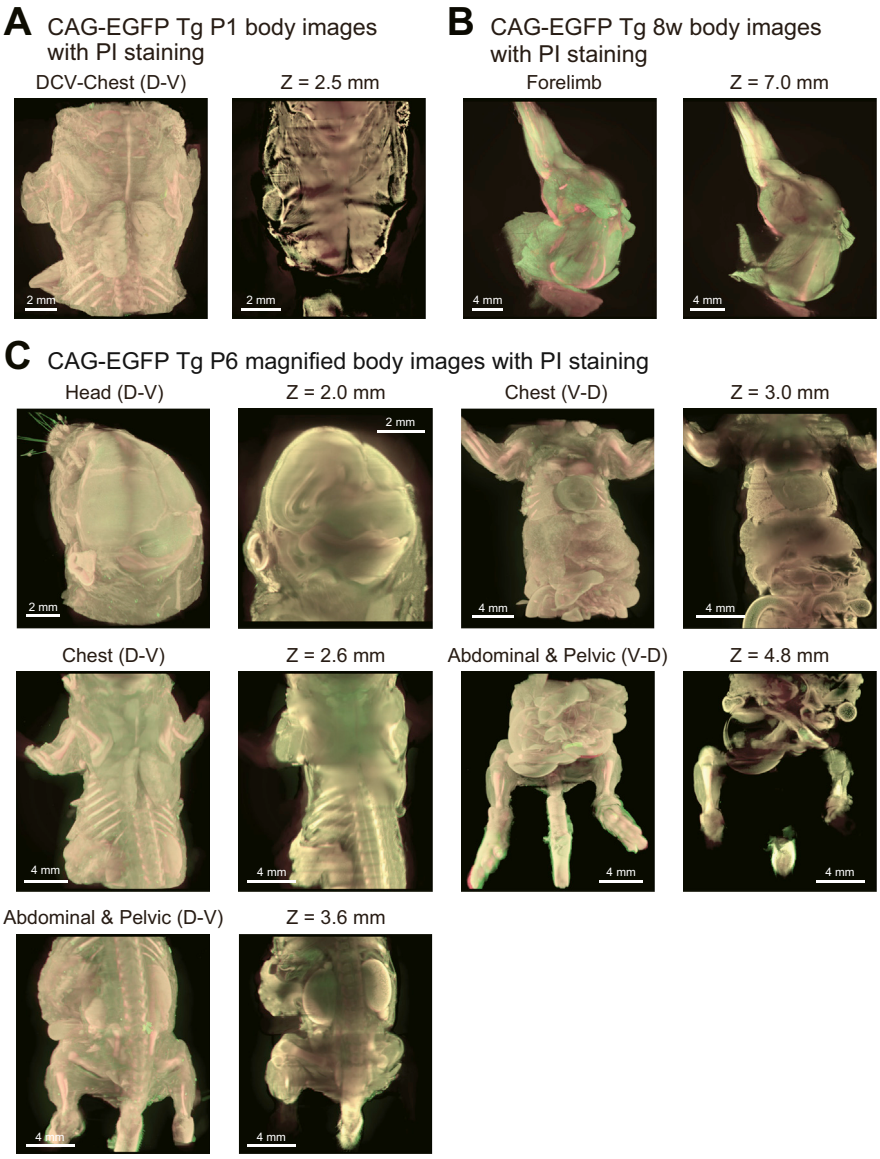

Figure S3. CUBIC Is Applicable to Whole-Body Imaging of Infant and Adult Mice with Single-Cell Resolution, Related to Figure 3

(A) 3D-reconstituted and X-Y plane body images of PI-stained CAG-EGFP Tg P1 mouse. Chest organs (D-V) are shown. The image was deconvolved with AutoQuant X3 software. Z-stack: 20-μm step, with 4.0 s × two illuminations for EGFP and with 0.1 to 0.15 s × two illuminations for PI. Zoom of the microscope: 2.0 × . Prefix "DCV-" indicates the deconvolved image.

(B) 3D-reconstituted and X-Y plane body images of the PI-stained CAG-EGFP Tg adult mouse (8-week-old). Forelimb is shown. Z-stack: 20-μm step, with 0.4 to 2.0 s × two illuminations for EGFP and with 0.1 to 0.2 s × two illuminations for PI. Zoom of the microscope: 0.8 × .

(C) 3D-reconstituted and X-Y plane (indicated with Z position) body images of the PI-stained CAG-EGFP Tg P6 mouse. Head (D-V), chest organs (V-D and D-V), abdominal and pelvic organs (V-D and D-V) are shown. Z-stack: 20-μm step, with 4.0 s × two illuminations for EGFP and with 0.1 s × two illuminations for PI. Zoom of the microscope: 1.25 × except 2.0 × for head D-V image.

Figure S4. Magnified Organ Images of CAG-EGFP Tg P1 Mouse, Related to Figure 3

3D-reconstituted magnified organ images (submaxillary gland, heart, lung, stomach, liver, kidney, intestine, spinal cord, scrotum, and leg) of the PI-stained CAG-EGFP Tg P1 mouse were acquired with LSFM. All images were deconvolved with AutoQuant X3 software. Z-stack: 20-μm step, with 4.0 s × two illuminations for EGFP and with 0.1 to 0.2 s × two illuminations for PI. Zoom of the microscope: 5.0 × . Note that the structures inside the spiral canal or leg bones were detected (panels of spinal cord and leg). Prefix "DCV-" indicates the deconvolved image.

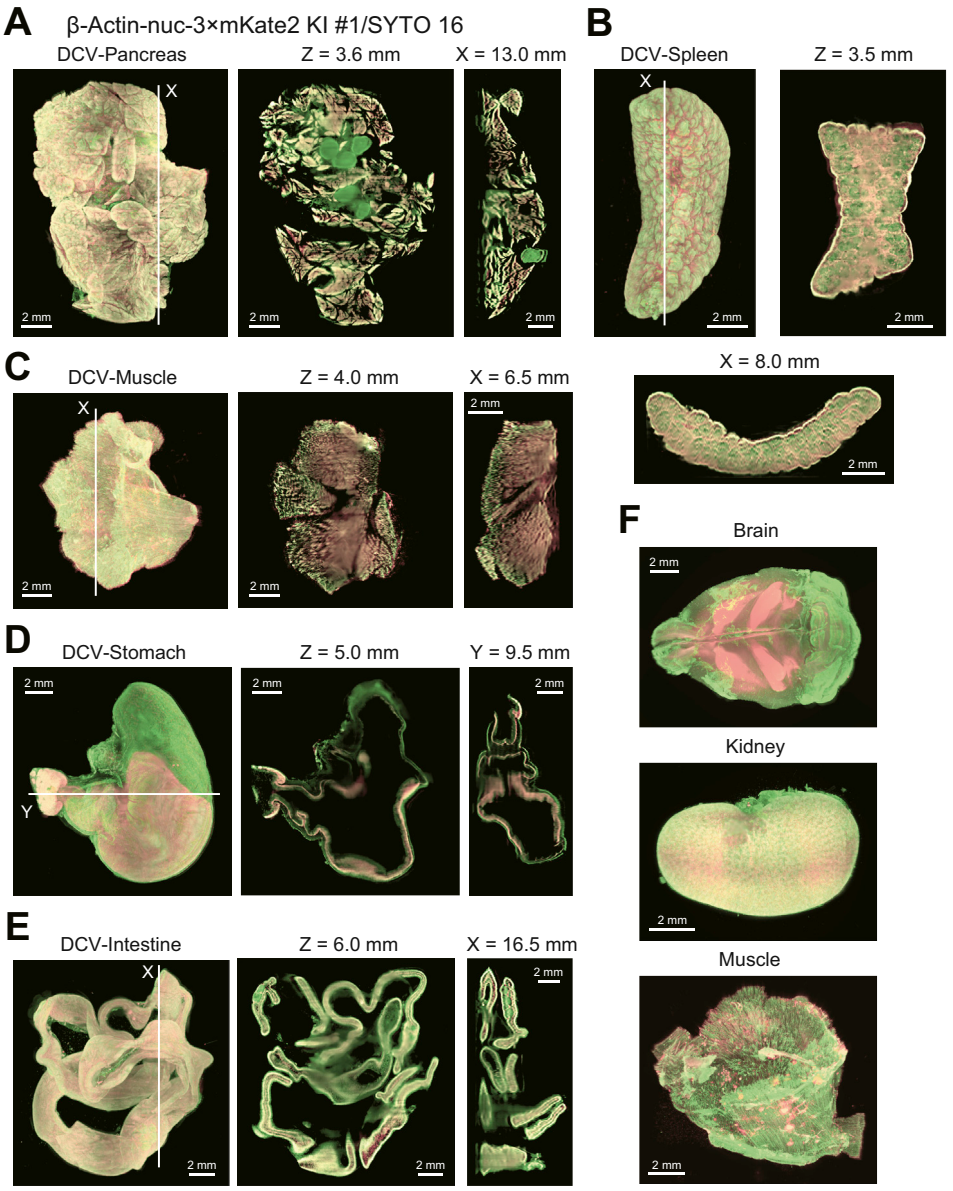

Figure S5. CUBIC Is Applicable to Whole-Organ Imaging with Single-Cell Resolution, Related to Figure 4

(A–F) The reconstituted 3D and section images of the SYTO 16-stained mouse pancreas (A), spleen (B), soleus muscle (C), stomach (D), intestine (E), brain, another kidney (contralateral to the kidney shown in Figure 4C), and another soleus muscle (contralateral to the soleus muscle shown in Figure S5C) (F), of β-actin-nuc-3 × mKate2 KI mouse (8-week-old) were acquired with LSFM. In (A)-E, images were deconvolved with AutoQuant X3 software. Raw X-Y section images, and reconstituted Y-Z and X-Z section images are at the indicated positions.

(A) Pancreas images. Z-stack: 20-μm step × 321 planes, with 0.05 s × two illuminations for SYTO 16 and with 0.5 s × two illuminations for mKate2. Zoom of the microscope: 1.25 × .

(B) Spleen images. Z-stack: 20-μm step × 231 planes, with 0.05 s × two illuminations for SYTO 16 and with 1.0 s × two illuminations for mKate2. Zoom of the microscope: 1.6 × .

(C) Soleus muscle images. Z-stack: 20-μm step × 331 planes, with 0.10 s × two illuminations for SYTO 16 and with 2.0 s × two illuminations for mKate2. Zoom of the microscope: 1.6 × .

(D) Stomach images. Z-stack: 20-μm step × 396 planes, with 0.05 s × two illuminations for SYTO 16 and with 1.0 s × two illuminations for mKate2. Zoom of the microscope: 1.25 × .

(E) Intestine images. Z-stack: 20-μm step × 366 planes, with 0.05 s × two illuminations for SYTO 16 and with 2.0 s × two illuminations for mKate2. Zoom of the microscope: 1.0 × .

(F) The reconstituted 3D images of brain, contralateral kidney, and contralateral muscle. Zoom of the microscope: 1.25 × for brain, 2.0 × for kidney, and 1.6 × for muscle. Prefix "DCV-" indicates the deconvolved image.

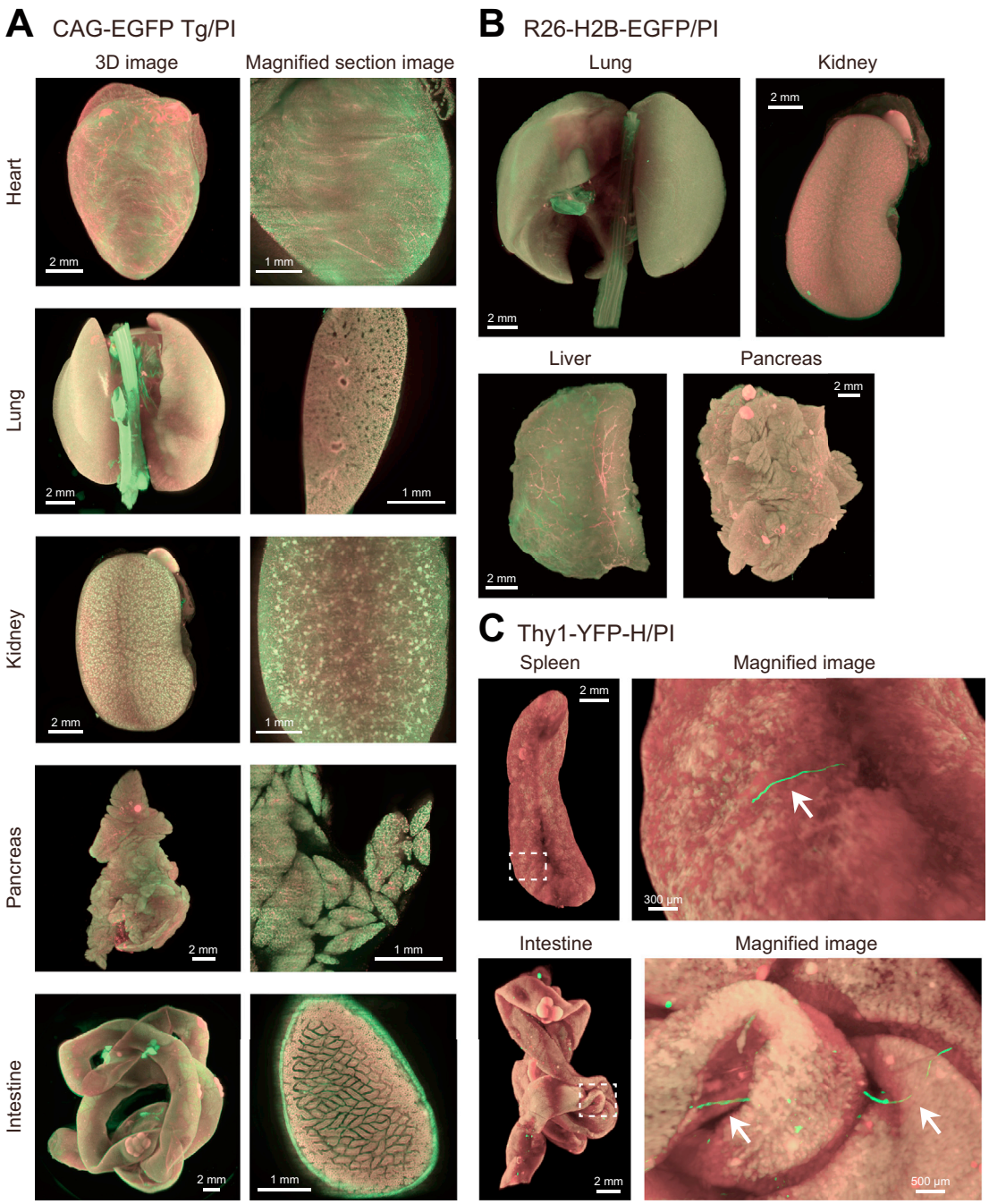

Figure S6. CUBIC Is Applicable to the Whole-Organ Imaging of Various Fluorescent Proteins, Related to Figure 4

(A) The reconstituted 3D whole-organ and magnified section images of heart, lung, kidney, pancreas, and intestine from CAG-EGFP Tg mouse (8-week-old) were acquired with LSFM. The magnified section images of EGFP/PI merged signals at the approximate 1 mm depth of each organ. Z-stack: 20-μm step, with 0.3 to 2.0 s × two illuminations for EGFP and with 0.1 to 0.4 s × two illuminations for PI. Zoom of the microscope: 0.8 × for intestine, 1.0 × for pancreas, 1.25 × for lung, 1.6 × for heart and kidney, and 5.0 × for all magnified section images.

(B) The reconstituted 3D whole-organ images of lung, kidney, liver, and pancreas from R26-H2B-EGFP KI mouse (4-month old) were acquired with LSFM. Z-stack: 20-μm step, with 2.0 s × two illuminations for EGFP and with 0.1 to 0.3 s × two illuminations for PI. Zoom of the microscope: 1.0 × for pancreas, 1.25 × for lung, liver, and kidney.

(C) The reconstituted 3D whole-organ images of spleen and intestine from Thy1-YFP-H Tg mouse (8-week-old) were acquired with LSFM. Z-stack: 20-μm step, with 0.7 to 2.0 s × two illuminations for YFP and with 0.1 to 0.3 s × two illuminations for PI. Zoom of the microscope: 0.8 × for intestine and 1.25 × for spleen. Magnified 3D images are at the indicated positions. Arrow indicates neurons.

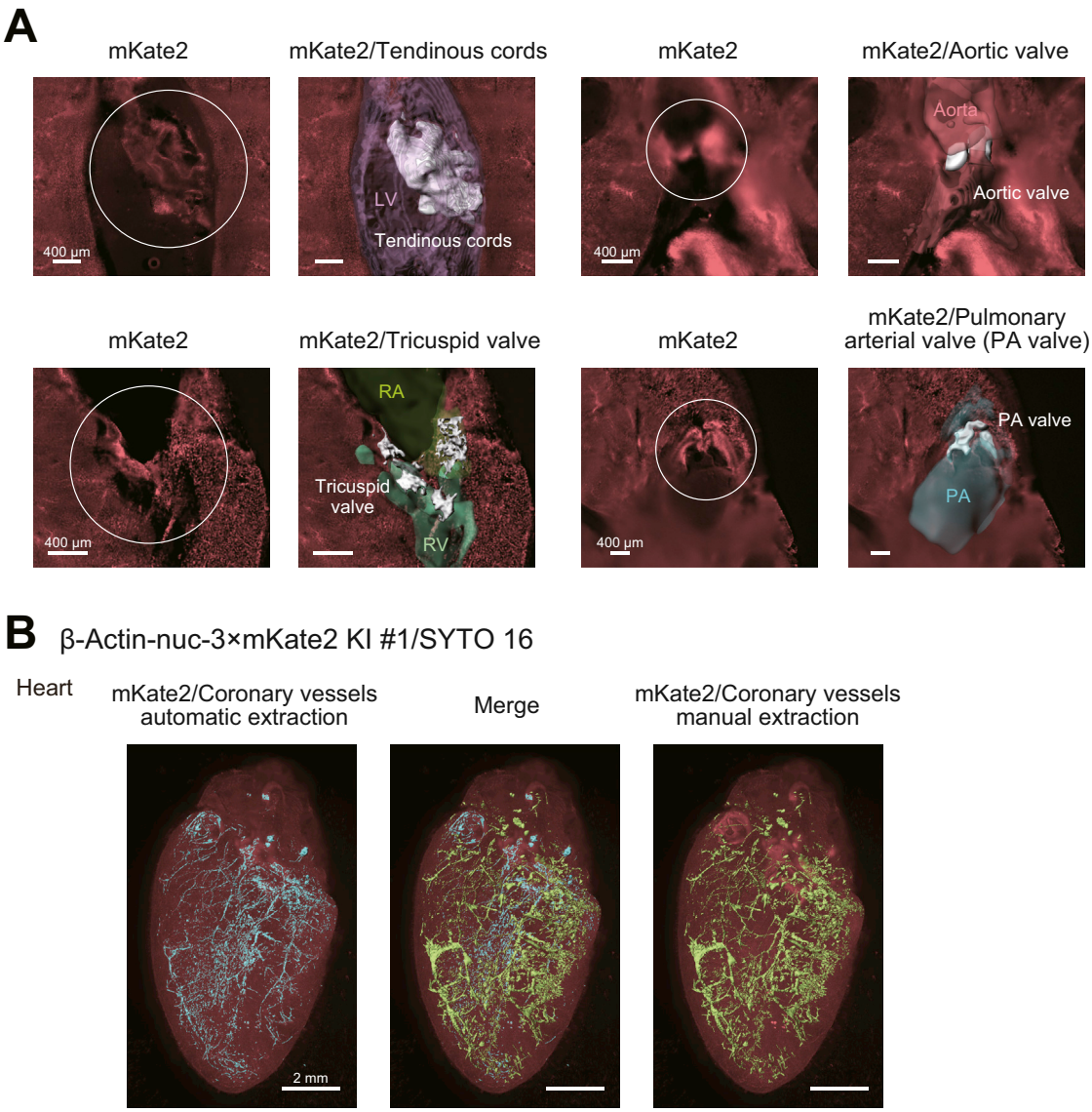

Figure S7. CUBIC Is Applicable to the 3D Anatomy of Organs, Related to Figure 6

Manual extraction of internal structures was performed with Surface analysis of Imaris software. The reconstituted 3D images of the heart from the SYTO 16-stained β-actin-nuc-3 × mKate2 KI mouse (8-week-old) in Figure 4 were used. After Surface extraction by the software, each structure was manually curated and extra Surface signals were eliminated.

(A) Detailed views of heart valves and surrounding structures. Cross sectional mKate2 images and surrounding structures (Surface volume, 3D) are shown.

(B) Automatic identification of coronary vessels. Left panel: automated extraction of coronary vessels with Fiji-based pipeline. Right panel: manual extraction of coronary vessels with Imaris in Figure 6A (view from different direction). Extracted vessels with these two methods are merged in the center panel.

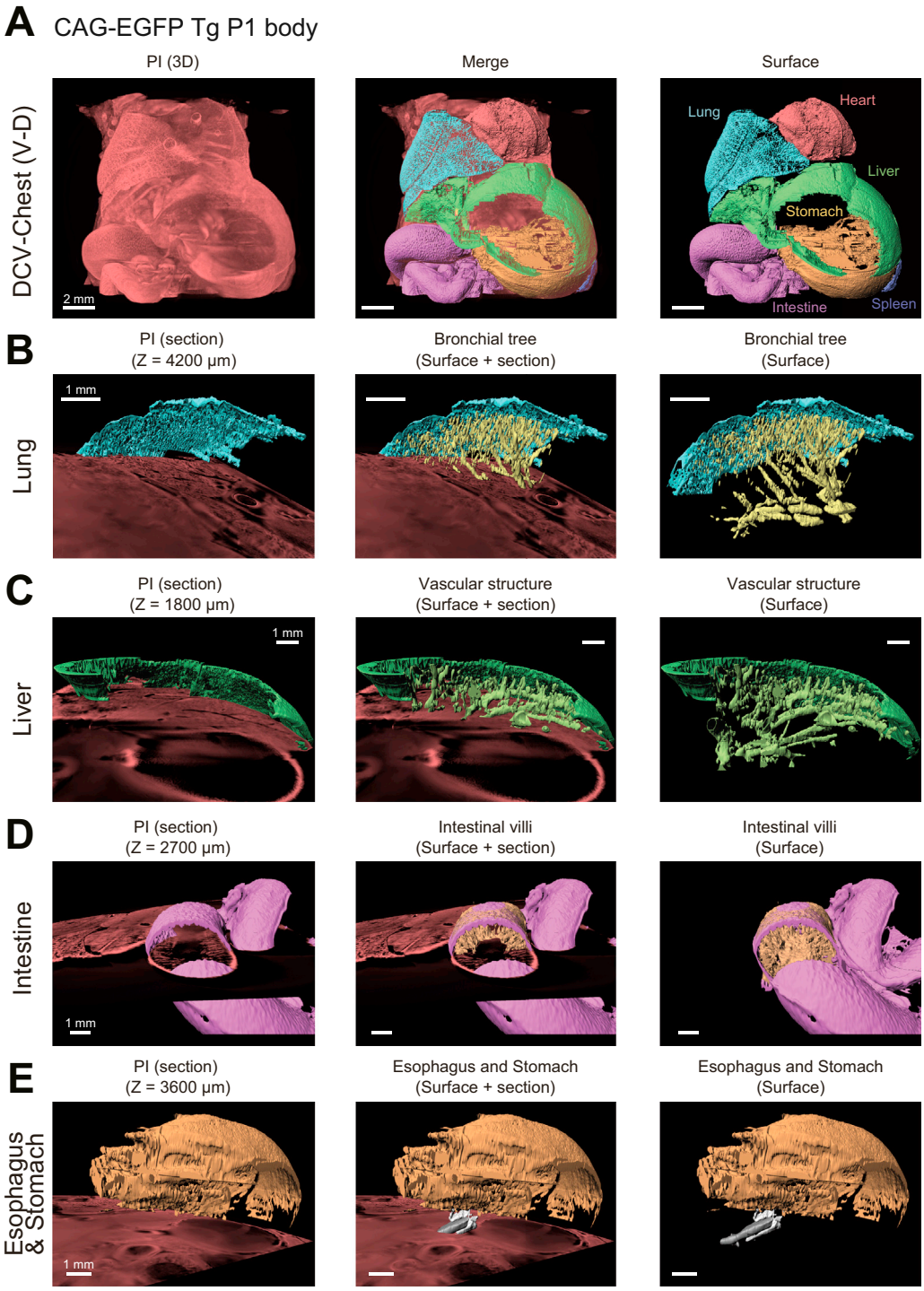

Figure S8. CUBIC Is Applicable to the 3D Anatomy of Infant Body, Related to Figure 6

(A–E) Extraction of internal structures was performed with surface analysis of Imaris software, similar in Figure 6. The reconstituted 3D images of the chest (A), lung (B), liver (C), intestine (D), and esophagus and stomach (E) from the PI-stained CAG-EGFP Tg P1 mouse in Figure 3B were used. After surface extraction by the software, each structure was manually curated and extra surface signals were eliminated. (A) Overview of organ identification using the chest 3D image with single-cell resolution. Prefix "DCV-" indicates the deconvolved image. (B) – (E) Extraction and visualization of the bronchial tree (yellow) with organ surface (light blue) of lung in (B), vascular structure (olive) with organ surface (green) of liver in (C), intestinal wall (purple) and villi (peachpuff) in (D) and stomach (brown), esophagus (gray) and esophageal gland (light gray) in (E).